Available online at www.sciencedirect.com
SCIENCE DIRECT
Journal of Catalysis 238 (2006) 58–66
JOURNAL OF CATALYSIS
www.elsevier.com/locate/jcat

Synthesis, crystal structure and catalytic activity for C_3H_6 combustion of La–Sr–Cu–O–S with K_2NiF_4-type perovskite structure

Masato Machida *, Ken-ichi Ochiai, Kazuhiro Ito, Keita Ikeue

Department of Applied Chemistry and Biochemistry, Faculty of Engineering, Kumamoto University 2-39-1 Kurokami, Kumamoto 860-8555, Japan

Received 1 October 2005; revised 28 November 2005; accepted 28 November 2005

Available online 27 December 2005

Abstract

K_2NiF_4 perovskite-type oxide catalysts containing sulfur, $La_{2-x}Sr_xCuO_4S_y$ ($0 \leqslant x \leqslant 0.3$; $0 \leqslant y \leqslant 0.3$), were synthesized to study their crystal structure, reduction–oxidation property, and catalytic activity for the combustion of C_3H_6 in the presence of SO_2. Results of XRD, Rietveld analysis, TG, and XPS demonstrated that sulfur is located in the interstitial site between perovskite slabs as nonsulfate species (S^{4+}/S^{6+}). Because of the high positive valence of sulfur in the lattice, resulting charge compensation decreased the oxidation number of Cu from 2.08 ($y = 0$) to 1.86 ($y = 0.2$), accompanied by the creation of more reducible Cu species in TPR profiles, which would achieve the light-off of catalytic C_3H_6 combustion at lower temperatures. Admission of SO_2 into the feedstream caused either a negative or a positive effect on the catalytic C_3H_6 oxidation, depending on the concentrations of SO_2 and O_2. More significantly, however, activation in the presence of SO_2 was observed for sulfur-containing compound ($y = 0.2$), which suppressed the accumulation of adsorbed SO_2 as sulfate (SO_4^{2-}). It is proposed that the adsorption of SO_2 leads to either positive or negative effects on catalytic activity depending on the oxidation state. The sulfur-containing compounds on exposure to SO_2 would create the surface active site effective for the adsorption and combustion of C_3H_6.

Keywords: Perovskite; Sulfur; SO_x; Crystal structure; Catalytic combustion

1. Introduction

Metal oxides with the perovskite-type structure have been studied as alternatives to noble metal catalysts for automotive exhaust purification since the 1970s [1–7]. The most serious problem in the application is deactivation due to sulfur (SO_2) poisoning [6,8]. Compared with noble metals, base metal oxides are more susceptible to sulfur poisoning. This is explained by the fact that SO_2 molecules adsorb strongly onto the metal and oxygen sites responsible for the catalytic conversion of CO and hydrocarbons, respectively. FTIR and XPS studies pointed out that the formation of $–SO_2$ and $–OSO_2$ would inhibit the adsorption of any other gases [9,10]. In many cases of perovskite-related oxides, a high basicity of A-site metals would also undergo a strong interaction with SO_2, which often results in structural destruction and simultaneous formation of sulfates [8]. As predicted by the thermodynamics, these solid–gas reactions between SO_2 and perovskite oxides to form sulfates cannot be avoided in a wide temperature range. Several attempts have been made to overcome this problem by introducing Ru or Pt oxide (which are less sensitive to SO_2 poisoning [11–13]) and MgO as a preferential adsorption site for SO_2 [14], or by seeking sulfur-bearing catalyst compositions [9,15,16]. Nevertheless, the development of SO_2-resistant perovskite catalysts remains unsolved.

To achieve this, we need a catalyst design that allows weaker interactions with SO_2. Based on this concern, we are interested in the sulfur-containing perovskite oxides as SO_x-resistant catalysts, because the driving force in sulfate formation is expected to be less than that of conventional oxides. The literature reports a few related materials in a series of studies directed toward high-temperature superconducting materials in the 1990s [17–19]. One example is in the K_2NiF_4-type cuprate system, $La_{1.85}Sr_{0.15}Cu_{1-x}O_{4-x}(SO_4)_x$, in which sulfur is considered present in the form of sulfate ions (SO_4^{2-}) substituting ca. 10% of the Cu site [17]. Another compound,

* Corresponding author.
E-mail address: machida@chem.kumamoto-u.ac.jp (M. Machida).

0021-9517/$ – see front matter
doi:10.1016/j.jcat.2005.11.040

$Ba_4MCu_{2+x}O_{6+y}(SO_4)_z$ (M=Ca, Y), which was also reported to contain SO_4 units substituting part of the Cu site in the structure, can accommodate larger amounts of sulfur, up to $z = 0.8$ [18]. Although these materials are thermally stable, their catalytic property and the role of sulfur have not been studied to date.

This paper focuses on such sulfur-containing K_2NiF_4-type perovskites presented by an empirical formula, $La_{2-x}Sr_xCuO_4S_y$. One objective is to study the effect of introducing sulfur on the crystal structure, reduction–oxidation properties, and catalytic activity. We measured their catalytic activity for combustion of C_3H_6, which is usually used as a model gas species for simulating vehicle exhaust. Another objective is to evaluate the sensitivity to SO_2 in the catalytic C_3H_6 combustion. Effects of SO_2 on catalytic activity are discussed with regard to the structure and surface reactivity of sulfur-containing catalysts.

2. Experimental

2.1. Catalyst preparation and characterization

Powder samples corresponding to apparent composition, $La_{2-x}Sr_xCuO_4S_y$ ($0 \leqslant x \leqslant 0.3$, $0 \leqslant y \leqslant 0.3$), were synthesized by calcining stoichiometric mixtures of La_2O_3, $SrCO_3$, CuO and $CuSO_4$ at 950 °C in air. Powder X-ray diffraction (XRD) measurements were performed on the product using monochromated Cu-K_α radiation (30 kV, 20 mA; Rigaku Multiflex). The X-ray structure analysis was carried out by the Rietveld method using the RIETAN-2000 profile refinement program [20]. The peak shape was described by a pseudo-Voigt function, and the background level was defined by a polynomial function. The scale factor, counter zero-point, peak asymmetry, and unit cell dimensions were refined in addition to the atomic parameters. Fitting between calculated and observed data was evaluated in terms of four agreement factors, R_{wp}, R_p, R_I, and R_F [21]. The sulfur content was determined by X-ray fluorescence (XRF) measurement (Horiba MESA500W). The XPS spectra were measured on a VG Sigmaprobe spectrometer using Al-K_α radiation (15 kV, 7 mA). The binding energy calculation was checked, using the line position of C1s as an internal reference. The charging effect was ruled out in the measurement, because the binding energy for C1s was identical for all the samples. The normal operating pressure in the analysis chamber was controlled at $<10^{-6}$ Pa during the measurement.

The reduction/reoxidation behavior was analyzed by temperature-programmed reduction and reoxidation (TPR/TPRO) in a conventional flow reactor connected to a differential evacuation system. After evacuation at ambient temperature, the sample (0.2 g) was heated in a flowing gas mixture of 10% H_2 and He (20 $cm^3\,min^{-1}$) at a constant rate (10 °C min^{-1}) up to 950 °C. Effluent gas from the sample was analyzed by a quadrupole residual gas analyzer mass spectrometer (Anelva M100). After the TPR measurement was completed, the sample was cooled slowly to ambient temperature in a stream of 10% H_2/He. This was followed by evacuation and the second heating in a flowing gas mixture of 5% O_2/He (20 $cm^3\,min^{-1}$) at a constant rate (10 °C min^{-1}) up to 950 °C, to measure TPRO profiles. To estimate the oxidation numbers of Cu and S, the reduction was also carried out in microbalance (TG, Rigaku 8120), which is connected to a gas supplying system. The sample (ca. 10 mg) was heated in a stream of H_2 at (20 $cm^3\,min^{-1}$) at a constant rate (10 °C min^{-1}) up to 950 °C. FTIR spectra were recorded on a Jasco FTIR-610 spectrometer. The sample was placed in a diffuse reflectance cell (Jasco DR600A), which was connected to a gas flow system. At resolution of 4 cm^{-1}, 512 scans were usually recorded. All spectra thereby obtained were transformed into absorption spectra using the Kubelka–Munk function.

2.2. Catalytic reactions

Total oxidation of C_3H_6 over catalysts was examined in a conventional flow reactor at atmospheric pressure. As-prepared sample (10–20 mesh, 0.20 g) was fixed in a quartz tube by quartz wool at both ends of the catalyst bed. So-called "light-off" characteristic was evaluated by heating the catalyst from room temperature to ca. 700 °C at a constant rate of 2 °C min^{-1} in a gaseous mixture of C_3H_6 (0.1%), O_2 (0.5 or 5%), and N_2 (balance) supplied at 100 $cm^3\,min^{-1}$ ($W/F = 0.002$ $g_{cat}\,min\,cm^{-3}$). The C_3H_6 conversion to CO_2 in the effluent gas was analyzed every 5 min by on-line gas chromatography (FID, molecular sieve 5A) equipped with a methanizer. Carbon dioxide was the sole reaction product observed over the whole temperature range. The sensitivity to SO_2 poisoning was evaluated during isothermal catalytic combustion of C_3H_6 at ca. 400 °C by adding 20 or 50 ppm SO_2 to the feedstream, C_3H_6 (0.1%), O_2 (0.5 or 5%), and N_2 (balance), supplied at 100 $cm^3\,min^{-1}$ ($W/F = 0.002$ $g_{cat}\,min\,cm^{-3}$. The adsorption of C_3H_6 onto the sample was evaluated in pulse mode reactions at 200 °C before and after exposure to the mixture of SO_2 (50 ppm), C_3H_6 (0.1%), O_2 (5%), and N_2 (balance) at 400 °C.

3. Results and discussion

3.1. Crystal structure of La–Sr–Cu–O–S

The XRF analysis indicated that as calcined solid products, $La_{2-x}Sr_xCuO_4S_y$ contained sulfur in a stoichiometric ratio. The effect of A-site composition ($0 \leqslant x \leqslant 0.3$) on the crystal structure of $La_{2-x}Sr_xCuO_4S_{0.2}$ was first studied using XRD. For all the x values, K_2NiF_4-type phases with a tetragonal $I4/mmm$ or an orthorhombic $Cmca$ space group were formed as a primary product, but impurities were formed depending on x. At low values of x ($\leqslant 0.2$), $La_2O_2SO_4$ and CuO were precipitated, whereas $SrSO_4$ and CuO appeared at higher x ($\geqslant 0.3$). Precipitation of these impurity phases would be originated from heterogeneous solid-state reactions between $CuSO_4$ and $SrCO_3/La_2O_3$ during calcination. The optimized composition was determined to be $x = 0.3$, where the least amount of impurities was observed. Fig. 1 shows the XRD patterns of $La_{1.7}Sr_{0.3}CuO_4S_y$ with different sulfur contents ($0 \leqslant y \leqslant 0.3$). The pristine compound ($y = 0$) contained a very small amount of $La_2SrCu_2O_6$, which disappeared after sulfur was introduced.

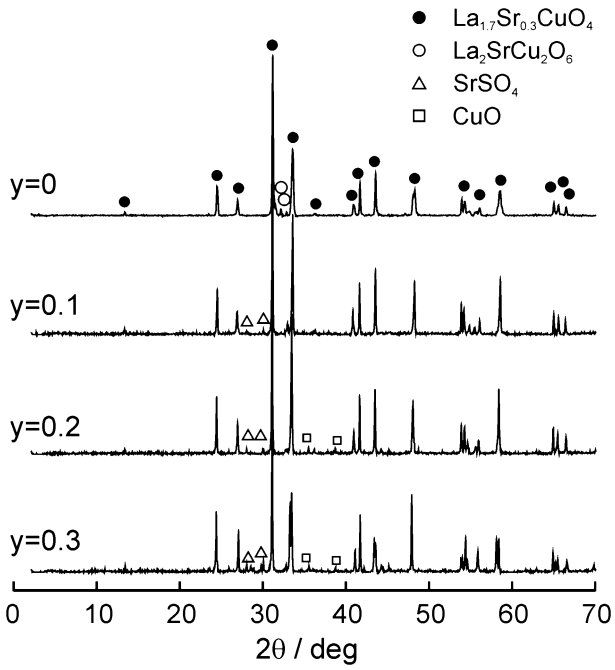

Fig. 1. XRD patterns of $La_{1.7}Sr_{0.3}CuO_4S_y$ after calcination at 950 °C.

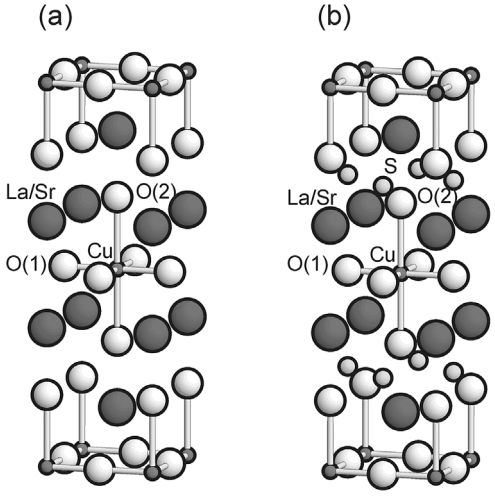

Fig. 2. Crystal structure models of (a) $La_{1.7}Sr_{0.3}CuO_4$ and (b) $La_{1.7}Sr_{0.3}CuO_4S_y$.

The amount of impurities ($SrSO_4$ and CuO) increased with increasing y, but the primary K_2NiF_4-type phase was preserved. Estimation from the intensities of individual peaks implies that ca. 50% of the sulfur in the starting material was deposited as $SrSO_4$, with the rest apparently incorporated into the perovskite structure. To determine the structural parameters of $La_{1.7}Sr_{0.3}CuO_4$ ($y = 0$), the Rietveld refinement method was applied to the dual-phase model because of the presence of $La_2SrCu_2O_6$. This gave agreement factors $R_{wp} = 12.2\%$, $R_p = 9.3\%$, $R_I = 2.6\%$, and $R_F = 2.3\%$ (Table 1). The resultant structural parameters are very similar to those reported by Lander et al. [22] for $La_{1.7}Sr_{0.3}CuO_4$ (*Cmca*, $a = 0.5350$ nm, $b = 1.3232$ nm, $c = 0.5333$ nm), in which La and Sr are distributed randomly in the $8f$ site (see the reduced cell in Fig. 2a).

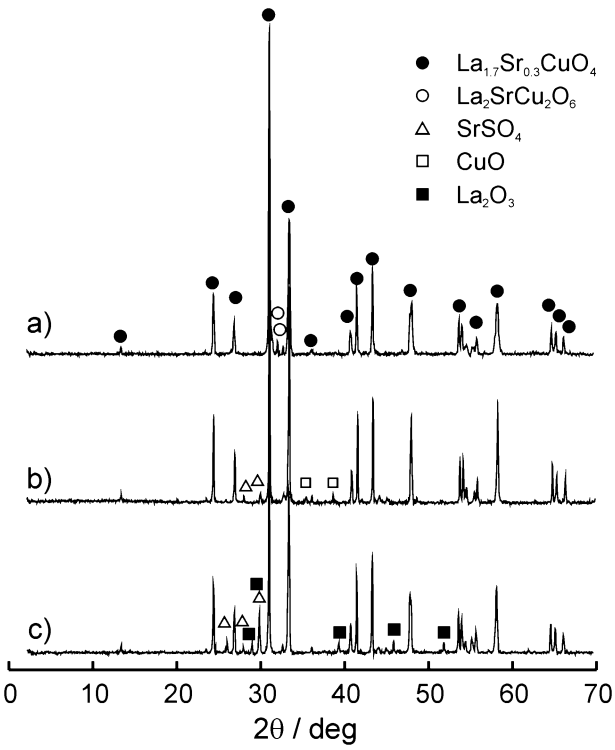

Fig. 3. XRD patterns of (a) $La_{1.7}Sr_{0.3}CuO_4$, (b) $La_{1.7}Sr_{0.3}CuO_4S_{0.2}$ and (c) $La_{1.7}Sr_{0.3}Cu_{0.8}O_4S_{0.2}$ after calcination at 950 °C.

For the samples containing sulfur, an initial structural model was adopted on the basis of assumption that the main lattice constructs a layered perovskite analogous to $La_{1.7}Sr_{0.3}CuO_4$. But the position of sulfur is not known. Concerning the crystal structure of sulfur-containing perovskite cuprates, the possibility of substituting sulfate ions into $La_{1.85}Sr_{0.15}CuO_4$ was reported by Greaves et al. [16]. Based on the X-ray emission spectroscopy and powder XRD analysis, these authors concluded that sulfur is present as SO_4^{2-} at the Cu site. Applying this model to the present system, the ideal composition must be expressed as $La_{1.7}Sr_{0.3}Cu_{1-y}O_4(SO_4)_y$. To ascertain this possibility, we tried to calcine the powder mixtures with the composition, $0.85\,La_2O_3{:}0.3\,SrCO_3{:}(1-2y)CuO{:}yCuSO_4$, at 950 °C. As shown in Fig. 3, however, the product with a nominal composition of $La_{1.7}Sr_{0.3}Cu_{0.8}O_4S_{0.2}$ (c) yielded more impurities ($SrSO_4$ and La_2O_3) than did $La_{1.7}Sr_{0.3}CuO_4$ (a) and $La_{1.7}Sr_{0.3}CuO_4S_{0.2}$ (b), because of the lack of Cu. Thus, we concluded that substituting SO_4 for the Cu site is not appropriate for the present system.

Here we propose a possible alternative structure of $La_{1.7}Sr_{0.3}CuO_4S_y$, as shown in Fig. 2b. In this model, cationic sulfur is positioned in an interstitial site (0.25, 0.25, 0.25) between two adjacent perovskite layers. The sulfur does not form an SO_4 unit, but is coordinated by four oxygens, O(2), of each CuO_6 octahedron. The Rietveld refinement was thus carried out using a triple-phase model containing $La_{1.7}Sr_{0.3}CuO_4S_y$ and two impurities ($SrSO_4$ and CuO). The observed, calculated, and difference diffraction profiles are shown in Fig. 4. The crystallographic data thus calculated for three compounds with $y = 0$, 0.1, and 0.2 are given in Table 1. The calcula-

Table 1
Crystallographic data of $La_{1.7}Sr_{0.3}CuO_4S_y$ ($y = 0$, 0.1 and 0.2)

	Atom	Site	g	x	y	z	B (nm^2)
				$y = 0$			
Cmca(No. 64)	La	8*f*	0.9289	0.0	0.36032(8)	0.0	0.003
$a = 0.53501(2)$ nm	Sr	8*f*	0.0711	0.0	0.36032(8)	0.0	0.003
$b = 1.32316(4)$ nm	Cu	4*a*	1.0000	0.0	0.0	0.0	0.003
$c = 0.53334(3)$ nm	O1	8*f*	1.0000	0.0050(5)	0.1827(7)	0.9764(53)	0.010
	O2	8*e*	1.0000	0.25	0.9875(16)	0.25	0.010
$R_{wp} = 12.20$ $R_p = 9.26$ $R_I = 2.63$ $R_F = 2.29$							
				$y = 0.1$			
Cmca(No. 64)	La	8*f*	0.9074	0.0	0.36029(8)	0.0	0.003
$a = 0.53352(2)$ nm	Sr	8*f*	0.0926	0.0	0.36029(8)	0.0	0.003
$b = 1.32392(4)$ nm	Cu	4*a*	1.0000	0.0	0.0	0.0	0.003
$c = 0.53282(4)$ nm	O1	8*f*	1.0000	0.0050(5)	0.1846(7)	1.0329(40)	0.010
	O2	8*e*	1.0000	0.25	0.9958(31)	0.25	0.010
	S	8*e*	0.0287	0.25	0.25	0.25	0.010
$R_{wp} = 12.74$ $R_p = 9.75$ $R_I = 3.55$ $R_F = 2.79$							
				$y = 0.2$			
Cmca(No. 64)	La	8*f*	0.8702	0.0	0.36088(7)	0.0	0.003
$a = 0.53489(2)$ nm	Sr	8*f*	0.1298	0.0	0.36088(7)	0.0	0.003
$b = 1.32098(3)$ nm	Cu	4*a*	1.0000	0.0	0.0	0.0	0.003
$c = 0.53440(2)$ nm	O1	8*f*	1.0000	0.0050(5)	0.1840(6)	0.9793(47)	0.010
	O2	8*e*	1.0000	0.25	0.9873(13)	0.25	0.010
	S	8*e*	0.0481	0.25	0.25	0.25	0.010
$R_{wp} = 10.90$ $R_p = 8.47$ $R_I = 3.62$ $R_F = 2.17$							

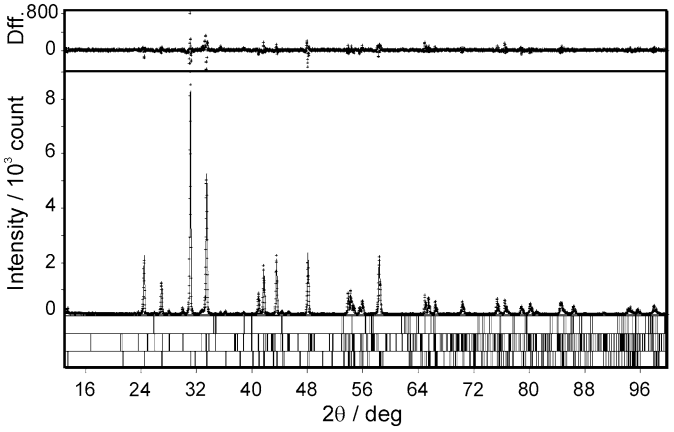

Fig. 4. Rietveld X-ray powder pattern fitting for $La_{1.7}Sr_{0.3}CuO_4S_{0.2}$. The difference between the calculated and observed patterns is shown on the top. The bottom bands display Bragg reflections for CuO (high), $SrSO_4$ (middle) and $La_{1.7}Sr_{0.3}CuO_4S_{0.2}$ (low).

tion for $y = 0.2$ gave rise to agreement factors ($R_{wp} = 10.9\%$, $R_p = 8.5\%$, $R_I = 3.6\%$, and $R_F = 2.2\%$) that are better than those for a model without sulfur. The optimized occupation factors, g, for S were 0.029 ($y = 0.1$) and 0.048 ($y = 0.2$), suggesting that ca. 57% ($y = 0.1$) and 48% ($y = 0.2$) sulfur of the nominal compositions can be introduced into the K_2NiF_4-type structure, whereas others should be precipitated as an impurity ($SrSO_4$). This is consistent with the result of XRD qualitative analysis mentioned above. Because the calculated S–O(2) bond length (0.21 nm) is much larger than that (0.15 nm) in a tetrahedral SO_4^{2-}, it does not change the local atomic arrangement and cell parameters. The structural model is consistent with various physicochemical properties, as described below, but it is still a possibility. Further details of the crystal structure are difficult to discern from the powder XRD data, because only very small amounts of sulfur can be incorporated into the perovskite unit. Structural analysis may require a neutron diffraction study.

3.2. Chemical state of sulfur

The structure of sulfur species was next studied using FTIR. Sulfur in the form of tetrahedral SO_4 provides two IR-active S–O stretching mode vibrations, ν_3 and ν_4 [23]. In many inorganic sulfates with a lower SO_4 symmetry, however, ν_1 and ν_2 appear in the spectrum. As shown in Fig. 5, bands at wavenumbers ca. 1100 (ν_3), ca. 1000 cm^{-1} (ν_1), and ca. 700 cm^{-1} (ν_4) were observed for a reference compound, $Ba_4YCu_{2.15}O_9(SO_4)_{0.8}$, the crystal structure of which was determined by neutron diffraction to contain a tetrahedral SO_4 unit [18]. In contrast, $La_{1.7}Sr_{0.3}CuO_4S_y$ ($0 \leqslant y \leqslant 0.3$) showed negligible absorption bands due to SO_4, in agreement with the structural model shown in Fig. 2b.

XPS measurements were performed to estimate the surface composition and chemical state of $La_{1.7}Sr_{0.3}CuO_4S_{0.2}$. Except for La, the calculated surface composition (La:Sr:Cu:S = 3.43:0.22:1:0.23) was close to the bulk composition (La:Sr:Cu:S = 1.7:0.3:1:0.2). Such enrichment of A-site metals is systematically found for many perovskite-related oxide catalysts, where several factors (including bulk composition, oxygen partial pressure, and temperature) are reported to influence the surface composition [24]. Figs. 6b–d show the S 2p spectra for the as-prepared sample with $y = 0.2$, demonstrating a broad anisotropic peak due to chemical inhomogeneity. A peak de-

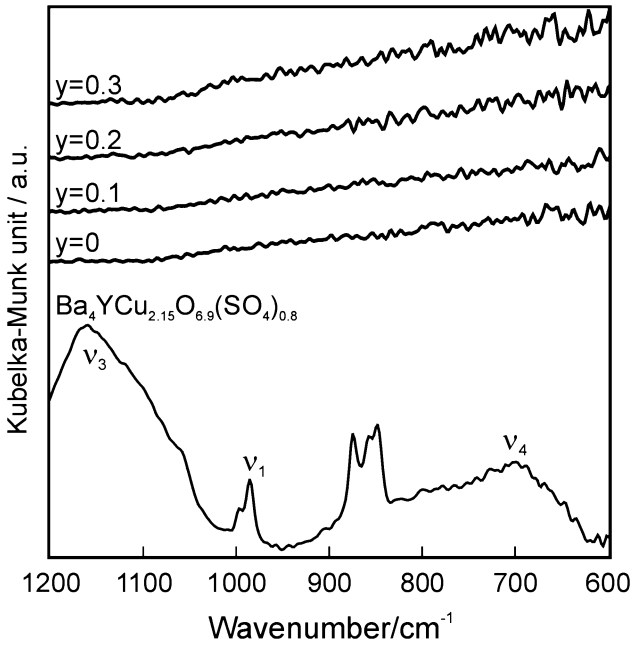

Fig. 5. FTIR spectra of $La_{1.7}Sr_{0.3}CuO_4S_y$ ($0 \leqslant y \leqslant 0.3$) and $Ba_4YCu_{2.15}O_{8.9}(SO_4)_{0.8}$.

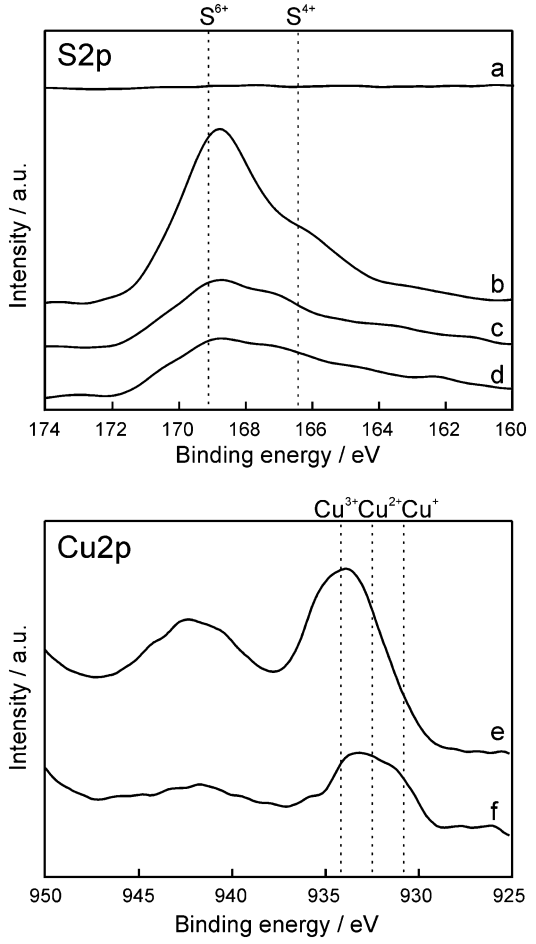

Fig. 6. S 2p XPS spectra of (a) $La_{1.7}Sr_{0.3}CuO_4$ and $La_{1.7}Sr_{0.3}CuO_4S_{0.2}$, (b) before and after Ar^+ etching for (c) 30 s and (d) 60 s. Cu 2p XPS spectra of (e) $La_{1.7}Sr_{0.3}CuO_4$ and (f) $La_{1.7}Sr_{0.3}CuO_4S_{0.2}$.

Table 2
Positive valence of Cu and S in $La_{1.7}Sr_{0.3}CuO_4S_y$

	$y = 0$	$y = 0.1$	$y = 0.2$
Cu valence	2.08	1.99	1.86
Cu per unit cell	1	1	1
S valence	–	4.77	3.97
S per unit cell	0	0.0574	0.0962
La valence	3	3	3
La per unit cell	1.858	1.815	1.740
Sr valence	2	2	2
Sr per unit cell	0.142	0.185	0.260
Total valence	7.94	8.07	7.98

The numbers of each atom per unit cell are obtained from the Rietveld refinement (Table 1).

convolution suggests the two peak maxima at 169 and 166.5 eV ascribable to S^{6+} and S^{4+}, respectively. The former species may be due in part to the impurity of $SrSO_4$. After Ar^+-bombardment for 60 s, however, the main peak at 169 eV became much less intense compared with the other peak at 166.5 eV. The corresponding S/Cu ratio on the surface decreased from 0.23 (0 s) to 0.12 (60 s), which is almost consistent with the occupation factor of S in the K_2NiF_4 structure (Table 1).

Another important effect on XPS caused by introducing S can be seen in the Cu 2p spectra shown in Figs. 6e,f. The Cu $2p_{3/2}$ spectrum of the pristine compound ($y = 0$, e) also showed a broad and anisotropic shape. One possible curve fitting provided three different components centered at ca. 931, 932.5, and 934 eV, which are assigned to Cu^+, Cu^{2+}, and Cu^{3+}, respectively. In contrast, for the sulfur-containing phase ($y = 0.2$, f), a peak at the lowest energy (931 eV) was intensified with a simultaneous decrease in a highest energy component (934 eV). The decreased Cu^{2+} concentration can also be deduced from shakeup satellite peaks at ca. 942 eV, which was weakened by introducing sulfur. These spectral changes can be rationalized by considering the charge compensation when sulfur with a high positive valence (S^{6+}/S^{4+}) occupies the interstitial site, as shown in Fig. 2b.

To confirm quantitatively the charge compensation mechanism, the TG measurement in a stream of H_2 was applied to $La_{1.7}Sr_{0.3}CuO_4S_y$ as summarized in Table 2. Here, the oxidation number of Cu and S in bulk samples can be determined from weight losses due to the reduction by H_2 to form Cu^0 and S^{2-}, which were observed at 300–500 °C and above 600 °C, respectively. The chemical composition of a K_2NiF_4-type phase was assumed to be equal to the occupation factor in Table 1. The oxidation numbers of La and Sr were fixed as 3+ and 2+, respectively, and the contributions from impurities ($CuO/SrSO_4$) were corrected. The weight loss due to the reduction of Cu decreased with an increase of y, as was observed in Cu 2p-XPS (Figs. 6). The calculated oxidation number of Cu decreased from 2.08 ($y = 0$) to 1.86 ($y = 0.2$), whereas the total positive valence remained nearly constant at ca. 8. The oxidation number of sulfur in the $La_{1.7}Sr_{0.3}CuO_4S_y$ phase was in the range of 4–5, in accordance with the S 2p-XPS (Figs. 6). Consequently, the incorporation of sulfur cations into a K_2NiF_4-type structure could be confirmed by the change in Cu oxidation number.

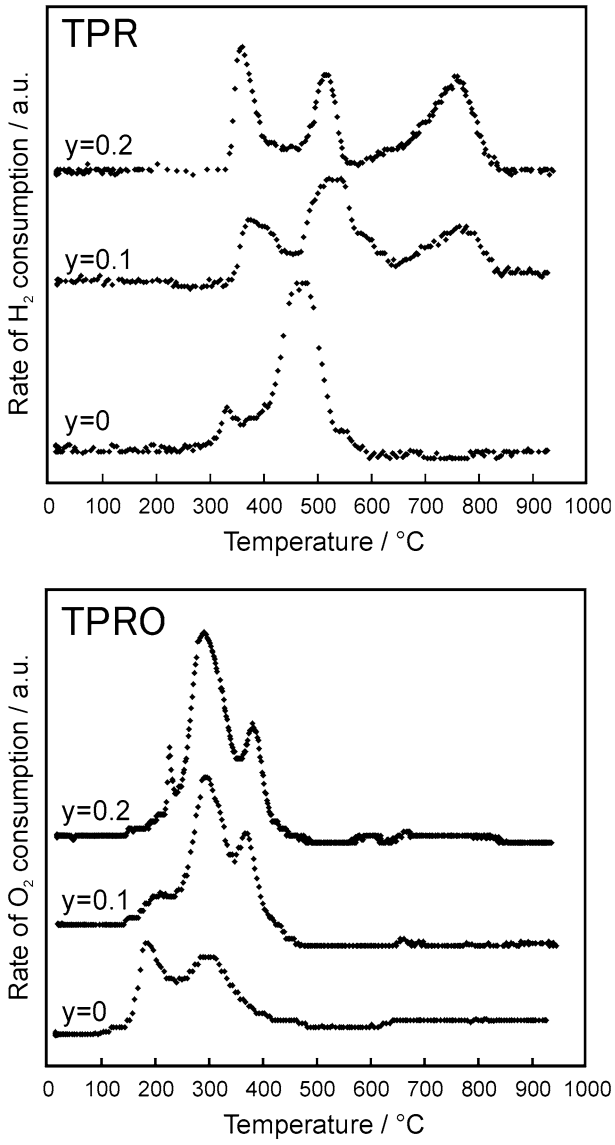

Fig. 7. TPR and TPRO profiles of $La_{1.7}Sr_{0.3}CuO_4S_y$ ($y = 0$, 0.1 and 0.2) measured in a stream of 10% H_2/He and 5% O_2/He, respectively. The catalyst was heated at a constant rate of 10 °C min^{-1}.

3.3. Reduction/oxidation property

The reduction/oxidation behavior of $La_{1.7}Sr_{0.3}CuO_4S_y$ was studied by means of a TPR/TPRO technique, as shown in Fig. 7. When the pristine compound ($y = 0$) was heated in a stream of 10% H_2/He, small and large peaks were observed at ca. 330 and 470 °C, attributed to the reduction of Cu^{3+} to Cu^{2+} and Cu^{2+} to Cu^0, respectively. For $y = 0.1$ and 0.2, however, the former peak disappeared and the latter peak was split into two peaks at ca. 350 and 500 °C. Note that the total area of these two peaks is less than that of the main peak of the pristine compound ($y = 0$), which also supports the decreased oxidation number of Cu. The appearance of the reduction peak at lower temperatures for $y = 0.1$ and 0.2 suggests that the perovskite-like phase became more reducible compared with the pristine compound ($y = 0$).

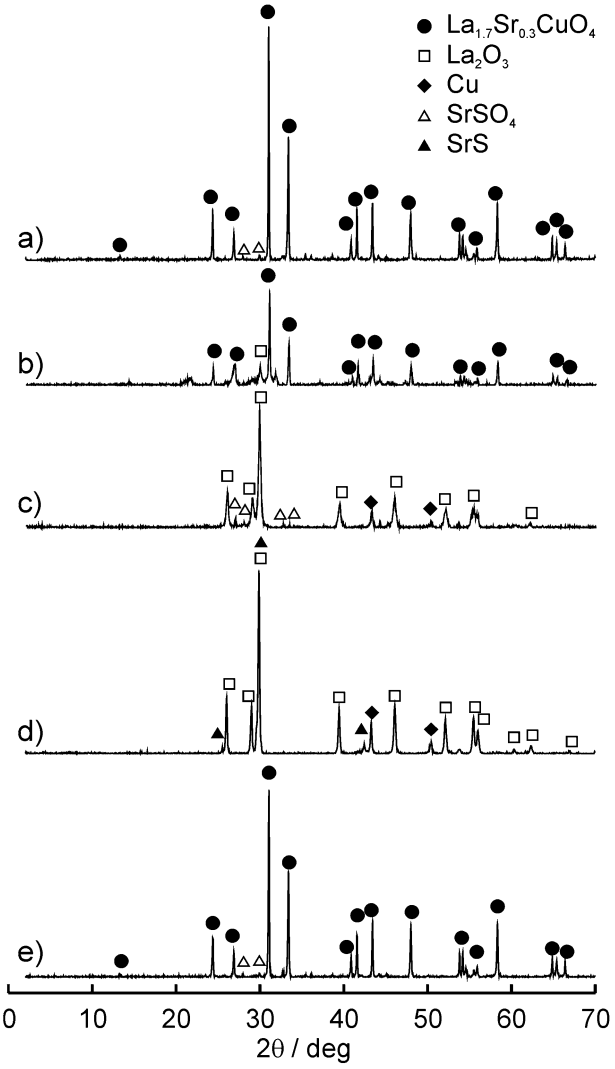

Fig. 8. XRD patterns of $La_{1.7}Sr_{0.3}CuO_4S_{0.2}$ (a) as prepared, after TPR up to (b) 350 °C, (c) 600 °C and (d) 950 °C, and (e) subsequent TPRO up to 950 °C.

Fig. 8 displays the change in XRD patterns ($y = 0.2$) during the course of TPR experiment. The first reduction peak at 350 °C was accompanied by partial collapse of the K_2NiF_4 phase (Fig. 8b). After completion of the second reduction step at $\leqslant$600 °C, the K_2NiF_4 phase was completely decomposed into mixtures of Cu, La_2O_3, and $SrSO_4$ (Fig. 8c). Intensified diffraction peaks due to $SrSO_4$ suggest that sulfur in the K_2NiF_4 structure was deposited as this phase. This was accompanied by the appearance of FTIR absorptions ascribable to the S–O stretching vibration of SO_4. These changes are compatible with the incorporation of sulfur into the K_2NiF_4-type lattice as a nonsulfate type species. Further heating thus gave rise to another TPR peak at $\geqslant$700 °C (Fig. 7), which is due to the reduction of $SrSO_4$ to SrS, as shown in Fig. 8d. After reduction, the sample was heated in a stream of 5% O_2/He to measure a reoxidation profile (TPRO). As shown in Figs. 7, the consumption of O_2 was completed at $\leqslant$500 °C, where the oxidation of Cu and SrS overlapped in a narrow temperature range, because these oxidation processes are thermodynamically favorable. After re-

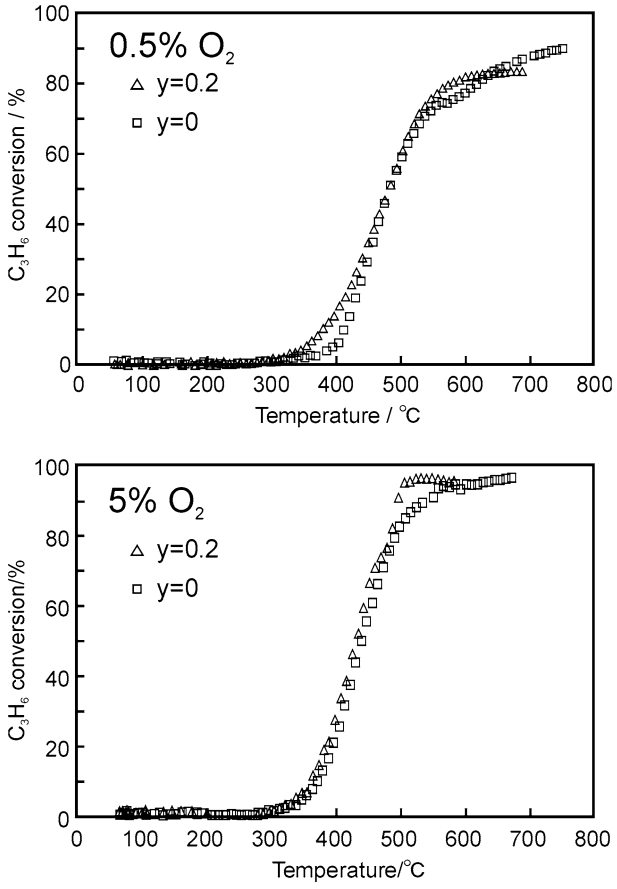

Fig. 9. Catalytic activity of $La_{1.7}Sr_{0.3}CuO_4S_y$ ($y = 0$ and 0.2) in a gaseous mixture of 0.1% C_3H_6, 0.5 or 5% O_2 and N_2 balance supplied at $W/F = 0.002$ $g_{cat}\,min\,cm^{-3}$. The catalyst was heated at a constant rate of $2\,°C\,min^{-1}$.

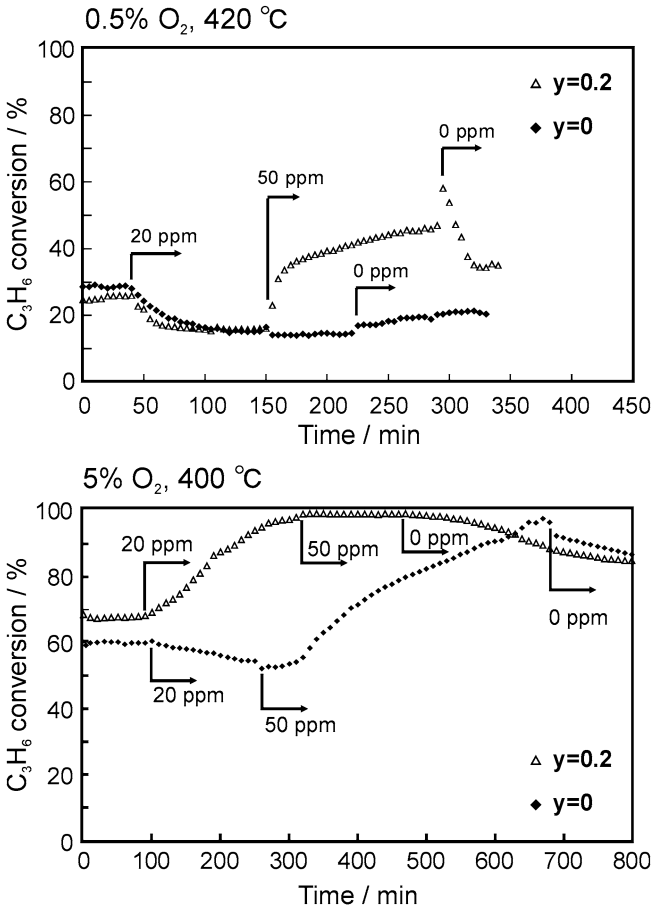

Fig. 10. Effect of SO_2 on catalytic C_3H_6 combustion over $La_{1.7}Sr_{0.3}CuO_4S_y$ ($y = 0$ and 0.2) in a gaseous mixture of 0.1% C_3H_6, 0.5 or 5% O_2 and N_2 balance supplied at $W/F = 0.002$ $g_{cat}\,min\,cm^{-3}$.

oxidation was completed, restoration of the initial K_2NiF_4-type structure was confirmed by XRD (Fig. 8e).

3.4. Catalytic properties

The catalytic activity for complete oxidation of C_3H_6 was evaluated in a conventional flow reactor (Fig. 9). The temperature dependence of C_3H_6 conversion in a large excess of O_2 (5%) suggested that the catalytic activity of two catalysts ($y = 0$ and 0.2) was comparable that and no deactivation was caused by introducing sulfur into the structure. However, the reaction in the presence of a small excess of O_2 (0.5%) gave rise to a little difference; that is, light-off was observed at $\leqslant$340°C for $y = 0.2$, compared with the temperature of ca. 400 °C required for $y = 0$. As shown in Fig. 7, the introduction of sulfur makes the Cu species more reducible than those in the pristine compound. This would lead to a smooth redox cycle at the low temperatures, a possible reason for the light-off at lower temperatures. The activity of S-containing catalyst was very stable, so that the conversion at 400 °C was kept almost constant for 50 h.

Another noticeable effect caused by sulfur in the structure was observed for the response to SO_2 in the gas feed. Fig. 10 compares the isothermal C_3H_6 conversion over pristine ($y = 0$) and sulfur-containing ($y = 0.2$) compounds at various O_2 concentrations. When 20 ppm of SO_2 was supplied at 0.5% O_2, the activity of both compounds decreased. However, the activity for $y = 0.2$ began to increase at 50 ppm SO_2, whereas that for $y = 0$ was still low. In the presence of a large excess of O_2 (5%), an activity increase became more obvious. On admission of 20 ppm of SO_2 into the feedstream, the conversion for $y = 0.2$ increased from 68 to >95%. Even for $y = 0$, activation was observed at 50 ppm of SO_2. When the SO_2 supply was turned off, the activity of both compounds slowly returned to the initial values, implying that the effect is reversible.

Enhanced activity was also confirmed for the sulfur-containing compound ($y = 0.2$) after treatment in a stream of 20 ppm SO_2, 5% O_2 balanced by N_2 for 2 h before the catalytic C_3H_6–O_2 reaction at 420 °C. This pretreated catalyst initially exhibited >90% conversion of C_3H_6, which slowly decreased to the steady-state conversion for the catalyst before the treatment (ca. 60%). In contrast, the activity of the pristine compound ($y = 0$) was decreased by this treatment. To increase the activity for $y = 0$, the treatment with >50 ppm of SO_2 seems to be necessary. These results suggest that the catalytic C_3H_6 combustion over the present system can be accelerated by SO_2, especially in the presence of excess O_2. This effect was more obvious for the sulfur-containing compound.

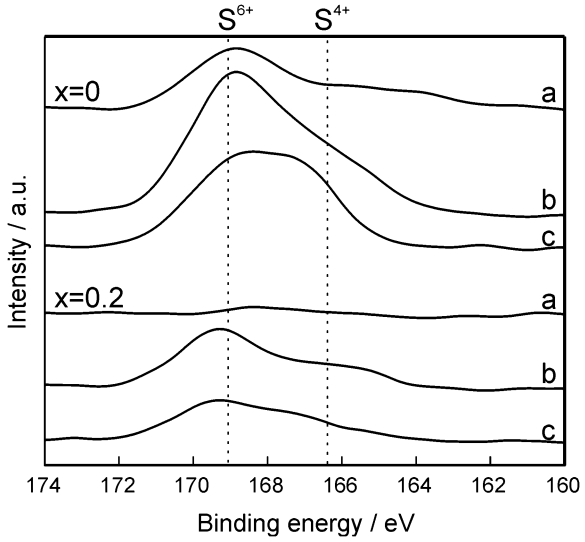

Fig. 11. XPS differential spectra of S 2p of $La_{1.7}Sr_{0.3}CuO_4S_y$ ($y = 0$ and 0.2) before and after exposure to (a) 20 ppm SO_2, 0.1% C_3H_6, 5% O_2 and N_2 balance, (b) 50 ppm SO_2, 0.1% C_3H_6, 5% O_2 and N_2 balance, and subsequently, (c) 0.1% C_3H_6, 5% O_2 and N_2 balance at 400 °C.

To elucidate the unusual response to SO_2 in excess O_2, characterization was done by XRD and XPS. No change was detected by XRD for both compounds ($y = 0$ and 0.2) after exposure to a reaction mixture containing SO_2. Fig. 11 shows the S 2p XPS differential spectra obtained by subtracting the spectra of as-prepared compounds from those after treatment at 400 °C. The catalyst without sulfur ($y = 0$, curve a) yielded signals at 169 eV ascribable to S^{6+} (SO_4^{2-}) on exposure to the reaction gas containing 20 ppm of SO_2 (a). This assignment was in agreement with FTIR spectra showing the appearance of ν_{SO} signals (at 1040 and 1090 cm^{-1}). When SO_2 was increased to 50 ppm (b), the signal intensified, and a shoulder due to S^{4+} appeared. On subsequent exposure to a mixture of C_3H_6 and O_2 (c), the S^{6+} signal was weakened, but S^{4+} remained strong. In contrast, the sulfur-containing compound ($y = 0.2$) exhibited a very small increase in the S 2p signal on exposure to SO_2. This clearly indicates that the sulfate-type adsorption of SO_2 can be prohibited by introducing sulfur into the perovskite structure, which is a plausible reason why the sulfur-containing sample is not deactivated by SO_2. Nevertheless, this cannot explain the increased activity observed in Fig. 10.

Considering that the concentration of SO_2 (20/50 ppm) in the gas feed is too low to cause the stoichiometric interaction with C_3H_6 (1000 ppm), the activation should be associated with the change in the catalyst surface caused by the interaction with SO_2. As is evident from Fig. 11, more S^{4+} species would be formed when both catalysts were activated by SO_2. Because most of the sulfur in the sample with $y = 0.1$ and 0.2 was in the form of S^{4+} (Table 2), this would not cause the deactivation. These results may indicate that the S^{4+} on the surface plays a key role in the activation process. Similar SO_2-induced activation effect on the catalytic oxidation over supported Pt catalysts has been reported by several research groups [25–30]. The effect seems to be reversible and is especially obvious for the oxidation of propane, whereas the reactions of propene and CO are inhibited by small amounts of SO_2. Yao et al. [25] initially reported that propane oxidation is promoted in the presence of SO_2 because of the formation of surface sulfate responsible for increased chemisorption of propane. To confirm this point, pulse reactions were conducted to measure the amount of C_3H_6 adsorption at 200 °C, where the catalytic reaction can be neglected. The as-prepared $y = 0$ compound exhibited negligible adsorption, whereas the sample exposured to SO_2 at 400 °C adsorbed 0.65 μmol g^{-1} of C_3H_6. The amount of C_3H_6 adsorption increased with increasing sulfur content (y). The fact that the BET surface area of $La_{1.7}Sr_{0.3}CuO_4S_y$ remained almost the same (ca. 0.3 $m^2\,g^{-1}$) irrespective of the sulfur content indicates that the interaction with C_3H_6 was affected not only by sulfur in the lattice, but also by preadsorbed SO_2. The results may support the proposal that adsorption of C_3H_6 is accelerated not only by introducing S^{4+} into the lattice, but also by adsorbed S^{4+} species. Clearly, more work is needed to understand the catalytic role of sulfur in the perovskite-type oxide catalysts and to develop a preparation route that can avoid the precipitation of impurities. Nevertheless, the results of the present study suggest that introducing a small quantity of sulfur causes a significant, more than expected, effect on the redox and catalytic properties.

4. Conclusion

A novel K_2NiF_4-type La–Sr–Cu–O–S perovskite has been synthesized and the crystal structure and catalytic properties have been studied. Structural and physicochemical analysis led to the development of a model of $La_{1.7}Sr_{0.3}CuO_4S_y$ in which cationic sulfur occupies the interstitial site between perovskite layers. Even though we could introduce only a small amount of sulfur into the perovskite structure ($y \leqslant 0.1$), the effects on the redox and catalytic properties were unexpectedly significant, because the large positive charge of sulfur requires a charge compensation by Cu species. The catalytic activity of sulfur-containing compounds for C_3H_6 combustion was as high as that of the pristine compound. But SO_2 adsorption onto the sulfur-containing compound, which was considerably less than that onto the pristine compound, produced the adsorbed species (S^{4+}) effective for enhanced adsorption and oxidation of C_3H_6.

Acknowledgments

This study was supported by a Grant-in-Aid for Scientific Research on Priority Area (440) from the Ministry of Education, Culture, Sports, Science and Technology (MEXT) and a Grant-in-Aid for Scientific Research (no. 16656250) from the Japan Society for the Promotion of Science.

Supplementary material

The online version of this article contains additional supplementary material.

Please visit doi: 10.1016/j.jcat.2005.11.040.

References

[1] W.F. Libby, Science 171 (1971) 499.
[2] R.J.H. Voorhoeve, J.P. Remeika, P.E. Freeland, B.T. Matthias, Science 177 (1972) 353.
[3] R.J.H. Voorhoeve, J.P. Remeika, D.W. Johnson, Science 180 (1973) 62.
[4] J.C. Schlatter, R.L. Klimisch, K.C. Taylor, Science 179 (1973) 797.
[5] R.J.H. Voorhoeve, in: J.J. Burton, R.L. Garten (Eds.), Advanced Materials in Catalysis, Academic Press, New York, 1977, p. 129.
[6] L.G. Tejuca, J.L.G. Fierro, J.M.D. Tascon, in: Advances in Catalysis, vol. 36, Academic Press, 1989, p. 237.
[7] T. Seiyama, in: L.G. Tejuca, J.L.G. Fierro (Eds.), Properties and Applications of Perovskite-Type Oxides, Dekker, New York, 1993, p. 215.
[8] L. Wan, in: L.G. Tejuca, J.L.G. Fierro (Eds.), Properties and Applications of Perovskite-Type Oxides, Dekker, New York, 1993, p. 145.
[9] P.G. Tsyrulnikov, O.N. Kovalenko, L.L. Gogin, T.G. Starostina, A.S. Noskov, Appl. Catal. A 167 (1998) 31.
[10] Y. Zhu, R. Tan, J. Feng, S. Ji, L. Cao, Appl. Catal. A 209 (2001) 71.
[11] M. Shelef, H.S. Gandhi, Platinum Met. Rev. 18 (1975) 8.
[12] L.E. Trimble, Mat. Res. Bull. 9 (1974) 1405.
[13] J.S. Croat, G.G. Tibbetts, Science 194 (1976) 318.
[14] I. Rosso, G. Saracco, V. Specchia, E. Garrone, Appl. Catal. B 40 (2003) 195.
[15] D. Klvana, J. Delval, J. Kirchnerova, J. Chaouki, Appl. Catal. A 165 (1997) 171.
[16] M. Alifanti, R. Auer, J. Kirchnoerova, F. Thyrion, P. Grange, B. Delmon, Appl. Catal. B 41 (2003) 71.
[17] H.M. Palmer, C. Greaves, M. Slaski, V.A. Trofimova, Y.M. Yarmoshenko, E.Z. Kurmaev, Physica C 291 (1997) 104.
[18] P.R. Slater, C. Greaves, Physica C 223 (1994) 37.
[19] S.M. Loureiro, P.G. Radaelli, E.V. Antipov, J.J. Capponi, B. Souletie, M. Brunner, M. Marezio, J. Solid State Chem. 121 (1966) 66.
[20] F. Izumi, T. Ikeda, Mater. Sci. Forum 321 (2000) 198.
[21] R.A. Young, in: R.A. Young (Ed.), The Rietveld Method, Oxford University Press, Oxford, 1993, Chapt. 1.
[22] G.H. Lander, P.J. Brown, C. Stassis, P. Gopalan, J. Spalek, G. Honig, Phys. Rev. B 43 (1991) 448;
M. Machkova, N. Brashkova, P. Ivanov, J.B. Carda, V. Kozhukharov, Appl. Surf. Sci. 119 (1997) 127;
P. Decorse, G. Caboche, L. Dufour, Solid State Ionics 117 (1999) 161.
[23] K. Nakamoto, Infrared and Raman Spectra of Inorganic and Coordination Compounds, 4th ed., Wiley, New York, 1986.
[24] N. Gunasekaran, N. Brakshi, C.B. Alcock, J.J. Carberry, Solid State Ionics 83 (1996) 145.
[25] H.C. Yao, H.K. Stepien, H.S. Gandhi, J. Catal. 67 (1981) 231.
[26] K. Wilson, C. Hardacre, R.M. Lambert, J. Phys. Chem. 99 (1995) 13755.
[27] A.F. Lee, K. Wilson, R.M. Lambert, C.P. Hubbard, R.G. Hurley, R.W. McCabe, H.S. Gandhi, J. Catal. 185 (1999) 491.
[28] J.T. Kummer, J. Phys. Chem. 90 (1986) 4747.
[29] J.W.A. Sachtler, I. Onal, R.E. Marinangeli, in: A. Crucq, A. Frennet (Eds.), Catalysis and Automotive Pollution Control, Elsevier, Amsterdam, 1987, p. 267.
[30] Y.F.Y. Yao, J. Catal. 36 (1975) 266.